Preliminary Observation of Nonlinear Effects in Compton Scattering ( )

C. Bula, K.T. McDonald and E.J. Prebys

Joseph Henry Laboratories, Princeton University, Princeton, NJ 08544

C. Bamber, S. Boege, T. Kotseroglou, A.C. Melissinos, D.D. Meyerhofer[(1)] and W. Ragg

Dept. of Physics and Astronomy, Dept. of Mechanical Engineering[(1)], University of Rochester, Rochester, NY 14627

D.L. Burke, R.C. Field, G. Horton-Smith, A.C. Odian, J.E. Spencer, D. Walz and M.S. Woods

Stanford Linear Accelerator Center, Stanford University, Stanford, CA 94309

S.C. Berridge, W.M. Bugg, K. Shmakov and A.W. Weidemann

Department of Physics and Astronomy, University of Tennessee, Knoxville, TN 37996

(July 20, 1995)

In a new experiment at the Final Focus Test Beam at SLAC a low-emittance 46.6-GeV electron beam is brought into collision with terawatt pulses from a 1.06-μm-wavelength Nd:glass laser. Peak laser intensities of 10^{18} W/cm^2 have been achieved corresponding to a value of 0.6 for the parameter $\eta = eE/m\omega_0 c$, and to a value of 0.3 for the parameter $\Upsilon = E^\star/E_{\mathrm{crit}} = 2\gamma e\hbar E/m^2 c^3$ in the case of frequency-doubled laser pulses. In these circumstances an electron that crosses the center of the laser pulse has near-unit interaction probability. Signals are presented for multiphoton Compton scattering in which up to 4 laser photons interact with an electron. High-energy backscattered photons of GeV energy can interact within the laser focus to create electron-positron pairs; an excess of 15 positrons above a background of 14 was observed in a run of 6,000 laser shots.

The interaction of electrons with intense wave fields was first considered by Schott [1] which led to the introduction of the dimensionless measure of field strength

$$\eta = \frac{eE_{\mathrm{rms}}}{m\omega_0 c} = \frac{eE_{\mathrm{rms}}\lambda_0/2\pi}{mc^2} = \frac{e\sqrt{\langle A_\mu A^\mu \rangle}}{mc^2},$$

for a plane wave of laboratory frequency ω_0, wavelength λ_0, electric field E and four-vector potential A_μ. A field with $\eta = 1$ has a voltage drop of an electron rest mass per reduced wavelength. In the average rest frame of an electron in a wave the transverse motion has characteristic velocity $\beta^\star = v^\star/c$ related by $\gamma^\star\beta^\star = \eta$, where $\gamma = 1/\sqrt{1-\beta^2}$, so that parameter η is often called v_{osc}/c in weak fields. As η approaches and exceeds unity the classical radiation spectrum includes higher harmonics of the wave frequency ω_0 (multipole radiation). In the quantum view this corresponds to absorption of several wave photons before emission of a photon of a frequency multiple of the wave:

$$e + n\omega_0 \rightarrow e' + \omega.$$

Only one observation of this effect has been reported: a weak signal of second-harmonic radiation in scattering of 1-keV electrons from a Q-switched Nd:YAG laser [2]. A closely related effect is higher-harmonic generation in a free-electron laser [3].

A quantum description of electrons in strong wave field utilizes the Volkov solutions [4,5] to the Dirac equation, in which an electron is 'dressed' by continual absorption and re-emission of wave photons leading to an effective mass

$$\overline{m} = m\sqrt{1 + \eta^2}.$$

The role of the effective mass in Compton scattering of electrons in a strong wave field was first discussed by Sengupta [6]; see also refs. [7-10]. In nonuniform waves the effective energy $\overline{m}c^2$ is called the ponderomotive potential, which describes the forces on a charged particle as it enters or exits the wave [11,12]. Ponderomotive effects on electrons ejected from atoms in a wave field with $\eta \approx 1$ have recently been observed by Moore *et al.* [13].
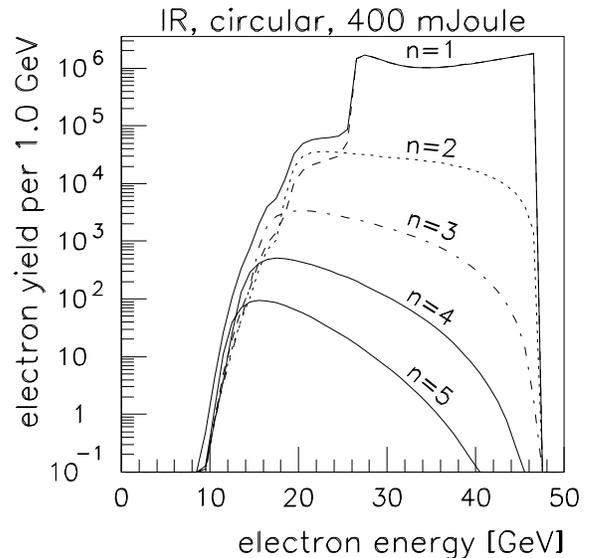

FIG. 1. Calculated yield of scattered electrons from the collision of 5×10^9 46.6-GeV electrons with a circularly polarized 1.06-μm laser pulse with intensity parameter $\eta = 0.5$.

Figure 1 shows the calculated spectra of scattered electrons in conditions representative of the present exper-

Submitted to the 1995 Lepton-Photon Symposium, Beijing, August 10-16, 1995

iment, following ref. [10]. The calculation includes the space-time profiles of the electron and laser beams and makes the adiabatic approximation that the theoretical rate based on infinite plane waves holds for the local value of η. The curve labeled $n = 1$ corresponds to ordinary Compton scattering, although the spectrum is rounded near the nominal endpoint of 25.4 GeV due to the larger effective mass of the electrons in the laser field. The spectra corresponding to absorption of more than one laser photon extend below 25.4 GeV, permitting a kinematic distinction between ordinary and nonlinear Compton scattering.

The dashed extension of the curve labeled $n = 1$ to energies below 25.4 GeV represents the background process in which an electron scatters from a sequence of laser photons at different space-time points. This process of multiple Compton scattering is also nonlinear in laser intensity, but is distinct from the process we call nonlinear Compton scattering in which several photons are absorbed at a single space-time point. Figure 2a represents $n = 2$ nonlinear Compton scattering, while Fig. 2b represents two successive ordinary Compton scatters. Electron e' in Fig. 2b is real. The black circles indicate that the absorption of a wave photon by an electron in a Volkov state is not simply described by a vertex factor of the charge e.
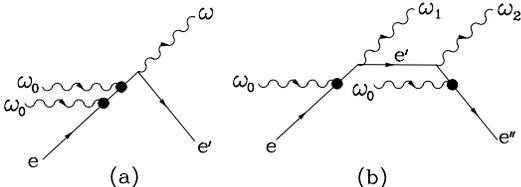

FIG. 2. Diagrams representing (a) $n = 2$ nonlinear Compton scattering, and (b) double Compton scattering.

In quantum electrodynamics a natural measure of electromagnetic field strength is the so-called critical field for which the voltage drop across a Compton wavelength is an electron rest mass:

$$E_{\rm crit} = \frac{m^2 c^3}{e\hbar} = 1.3 \times 10^{16} \ {\rm V/cm} = 4.4 \times 10^{13} \ {\rm gauss}.$$

The critical field was first introduced by Sauter [14] as the characteristic field strength at which Klein's paradox [15] becomes important and was further interpreted by Heisenberg and Euler [16] as the field strength at which electron-positron pair creation becomes copious. For a particle in a strong wave field a useful dimensionless invariant is

$$\Upsilon = \frac{e\hbar}{m^3 c^5}\sqrt{(F_{\mu\nu}p^\nu)^2} = \frac{E^\star}{E_{\rm crit}} = \frac{2\gamma E}{E_{\rm crit}},$$

where $F_{\mu\nu}$ is the field tensor and p_ν is the particle's 4-vector; $E^\star$ is the wave field in the particle's rest frame, and the final equality holds only if the particle is moving

anticollinear to the wave with Lorentz boost γ. Static fields with values of Υ approaching one are thought to exist at the surface of neutron stars. The field at the surface of a nucleus has Υ less than one, but quasistatic fields with Υ exceeding unity arise in MeV heavy-ion collisions.

Electron-positron creation can arise in the interactions of electrons with a wave in a two-step process in which a Compton-scattered photon collides with wave photons to produce the pair. Weak-field pair creation by photons was first considered by Breit and Wheeler [17], and Reiss [18] first discussed the strong-field case,

$$\omega + n\omega_0 \to e^+ e^-,$$

in which several wave photons participate; see also refs. [8] and [10]. Figure 3 represents the latter process for a case where an external photon and four wave photons combine to produce a pair.
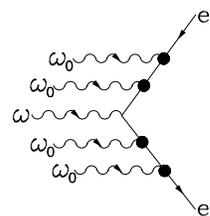

FIG. 3. Diagram representing multiphoton pair creation.

The present experiment studies the basic interactions of electrons and photons in fields near the QED critical field strength. It is also relevant to the understanding of so-called beamstrahlung processes at future e^+e^- colliders where the fields surrounding the beam bunches approach $E_{\rm crit}$ [19], and where the consequent pair creation will be a limiting background. The experiment provides a demonstration of the technology for e-γ and γ-γ collider options [20], leading to measurements of the γWW coupling via the reaction $e\gamma \to W\nu$ [21], $etc.$ Copious production of positrons in e-γ collisions can provide a low-emittance positron source due to the absence of final-state Coulomb scattering [22].

The parameters η and Υ are not independent, and for electrons colliding head-on with a wave their relation is $\Upsilon/\eta = 2\gamma\hbar\omega_0/mc^2$. For GeV electrons interacting with a laser the ratio of Υ to η is near one, so experiments in these conditions probe nonlinear effects due to both multiphoton absorption and vacuum polarization.

We report here on preliminary results of a study of strong-field QED in the collisions of 46.6-GeV electrons with 1.06- and 0.53-μm-wavelength photons at the SLAC Final Focus Test Beam. For this a new interaction point, IP1, was constructed 10 m downstream of the Final Focus as sketched in Fig. 4. The permanent dump magnets of the FFTB also served as the analyzing magnet of our experiment. Electrons scattered by the laser at IP1 and positrons produced there were detected in Si-W calorimeters.
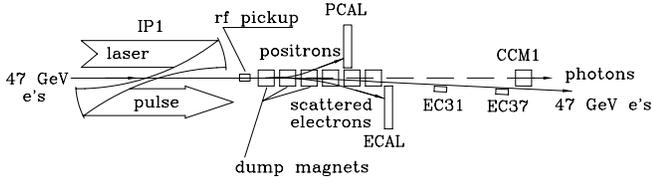
FIG. 4. Sketch of experiment E-144 to detect scattered electrons and positrons produced in e-laser collisions at the SLAC Final Focus Test Beam.

In the next phase of the experiment (Fig. 5) a thin foil or wire will convert high-energy Compton photons to pairs that will be analyzed in a pair spectrometer based on CCD's to reconstruct the photon-energy spectrum with resolution sufficient to discern the effective mass $\overline{m}$. In a third phase sketched in Fig. 6, part of the laser beam will collide with the high-energy Compton photons at a new interaction point, IP2, and the invariant mass of resulting pairs will be analyzed in the pair spectrometer free from backgrounds of electrons and positrons produced at IP1.
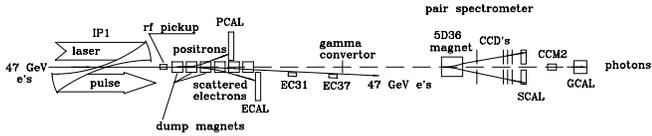

FIG. 5. Sketch of the experiment with the addition of a pair spectrometer to analyze converted Compton photons.
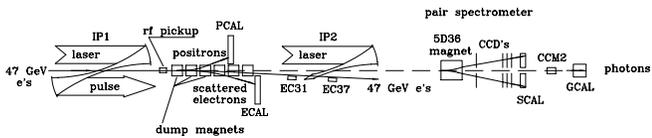

FIG. 6. Sketch of the experiment with the addition of a second laser interaction point to study pair creation by light.

The beam from a chirped-pulse-amplified terawatt Nd:glass laser system [23,24] is focused by off-axis-parabolic mirrors with a 17° crossing angle onto the electron beam at IP1. The laser system is shown in Fig. 7 and delivered pulses 1.5-ps (fwhm) wide at 0.5 Hz of up to 2 J of infrared light, or 1 J of green light after frequency doubling in a KDP crystal. The relatively high repetition rate is achieved in a final laser amplifier with slab geometry [25]. The laser-oscillator mode locker is synchronized to the 476-MHz drive of the SLAC linac klystrons via a rf/optical feedback system [26]. The observed jitter between the laser and linac pulses is 2 ps (rms) [27]. The laser-pulse energy, length and area are measured for each shot.

The peak focused laser intensity was obtained for infrared pulses of energy $U = 1.2$ J, focal area $A = 80$ μm^2 and pulse width $\Delta t = 1.5$ ps, for which $I = U/A\Delta t = 10^{18}$ W/cm^2 at $\lambda = 1.06$ μm, corresponding to a laboratory field of 20 GV/cm. The photon density at the laser

focus was 2×10^{26}/cm^3, some 30 times the electron density of gold. The field-intensity parameter η had a peak value of $6 \times 10^{-8}\lambda_0\sqrt{I} = 0.6$. The radiation length for electrons in a wave of strength $\eta \leq 1$ is $X_0 \approx 3\lambda_0/4\pi\alpha\eta^2$, where α is the fine structure constant. In our peak field, $X_0 \approx 95$ μm. The effective length of the laser pulse is $2\sqrt{A/\pi}/\sin 17° \approx 35$ μm. Thus electrons that passed through the focus of the laser at peak intensity had a 30% probability of interacting.
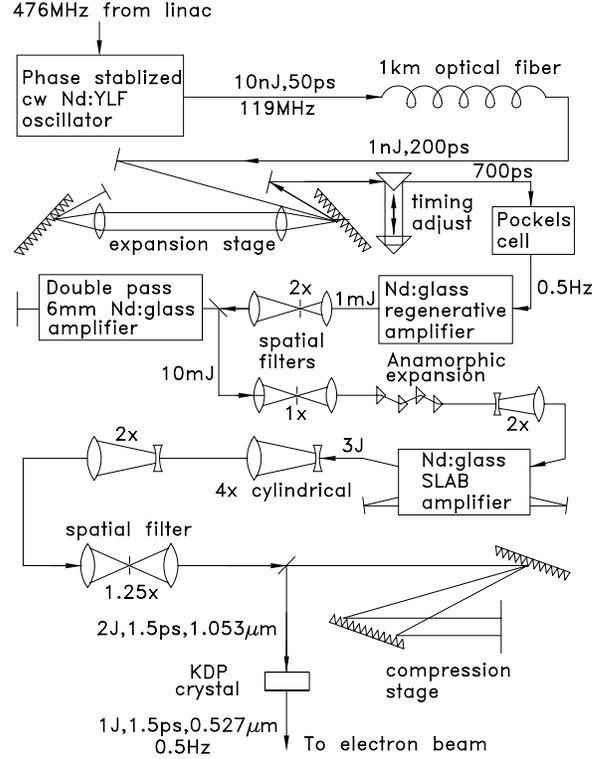

FIG. 7. Sketch of the terawatt Nd:glass laser system.

The Final Focus Test Beam (FFTB) [28] was operated at 10-30 Hz with an electron energy of 46.6 GeV and emittances $\epsilon_x = 3 \times 10^{-10}$ m-rad and $\epsilon_y = 3 \times 10^{-11}$ m-rad. The beam was retuned to a focus with $\sigma_x = 60$ μm and $\sigma_y = 70$ μm at interaction point IP1 some 10 m downstream of the final focus. The electron bunch length was expanded to 3.6 ps (rms) to minimize the effect of the time jitter between the laser and electron pulses. Typical bunches contained 5×10^9 electrons. Some data were taken with a new mode of linac operation in which pulses of as few as 10^7 electrons were transmitted at 1 Hz for 9 seconds, alternated with 30 Hz pulses of 5×10^9 electrons for 1 s while the linac feedback systems operated.

Compton-scattered electrons were deflected away from the primary electron beam by the dump magnets of the FFTB and detected in a silicon/tungsten calorimeter (ECAL) [29], sketched in Fig. 8a, that covered the range 10-30 GeV. Positrons were deflected to the opposite side of the electron beam where they could be detected in a similar calorimeter (PCAL). High-energy backscattered

3

photons were detected by monitor CCM1 which observed Čerenkov light from the conversion of the photons in 0.2 radiation lengths of aluminum, as sketched in Fig. 8b. Scattered electrons in the range 30-40 GeV were detected in Čerenkov monitors EC31 and EC37 of similar construction.
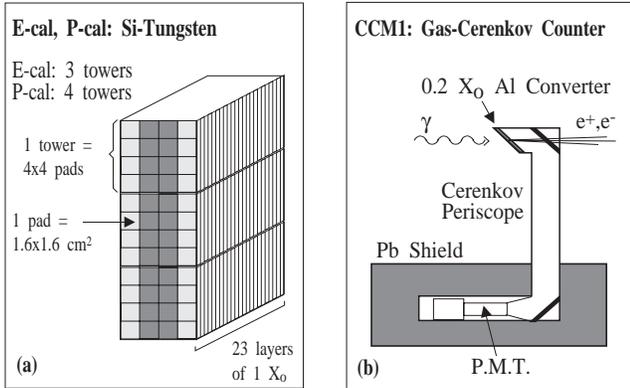

FIG. 8. (a) The silicon-tungsten calorimeters ECAL and PCAL. (b) The gas Čerenkov monitor CCM1; monitors EC31 and EC37 are of similar construction.

The silicon calorimeters were calibrated in parasitic running of the FFTB to the SLC program in which linachalo electrons of energies between 5 and 25 GeV were transmitted by the FFTB when tuned to a lower energy. The number of such electrons varied between 1 and 100 per pulse, which provided an excellent calibration of the ECAL and PCAL over a wide dynamic range. The calibration runs also yield a check of the maps of the FFTB dump magnets that are used in our spectrometer.
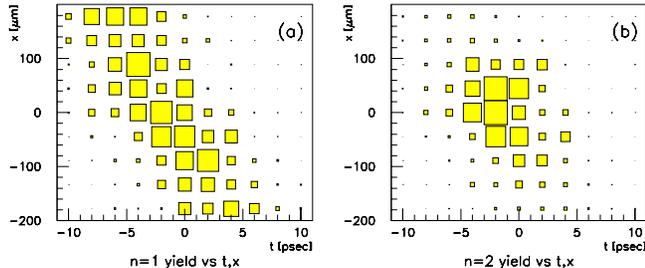

FIG. 9. Observed rates of (a) ordinary and (b) nonlinear Compton scattering as a function of x and t offsets between the electron and laser beams.

The spatial and temporal overlap of the electron and laser beams was monitored by observing the Compton scattering rate in the ECAL and CCM1 detectors during horizontal (x), vertical (y) and time (t) scans of one beam across the other. Figure 9 shows results of a combined x-t scan. The 17° beam-crossing angle leads to the observed slope to the data. Figure 9a is derived from scattered photons and is dominated by ordinary Compton scattering. Figure 9b is derived from electron of energy less than 25.4 GeV corresponding only to nonlinear Compton scattering. The space-time extent of Fig. 9b is less than that of Fig. 9a because the nonlinear process is more probable in the higher intensity regions of the laser beam.

In the commissioning of the present experiment in April 1994 a measurement was made of the longitudinal polarization of the electron beam. The result was $P_e = 0.81^{+0.04}_{-0.01}$ [30], in good agreement with measurements of the SLD collaboration. The upper error of 0.04 on the polarization is due to the uncertainty in the degree of circular polarization of the laser, and could readily be reduced to 0.01 in any future measurements.

The data concerning nonlinear Compton scattering were collected using the ECAL silicon calorimeter. It sampled 12 energy intervals each about 1.5 GeV wide. The highest energy sampled was 30 GeV, but the maximum sampled energy could be reduced by lowering the entire calorimeter away from the beam. When positioned with maximum energy below 25.4 GeV, only electrons from nonlinear scattering were detected. An ECAL channel saturated at 12 TeV, while at peak laser intensity some 10^7 Compton scatters occur per pulse. Hence the ECAL could not be used to study ordinary Compton scattering for laser intensities higher than about 0.001 of peak. Due to electronic crosstalk and backsplash from ordinary Compton-scattered electrons that hit the beampipe the dynamic range of ECAL was only about 100. A complete mapping of the nonlinear Compton spectrum required data collection at several laser intensities and positions of the ECAL.

Data were collected at 12 laser intensities, labelled by the corresponding laser pulse energies between 27 and 750 mJ, with a circularly polarized infrared beam. Figure 10 shows the observed rates $vs.$ scattered electron energy for three representative laser intensities, each normalized to the ordinary Compton rate as measured in the CCM1 photon monitor. Each data set utilized more than one ECAL position to permit finer energy steps and to explore the low-rate region better. Corrections for crosstalk and backsplash have been applied, based on algorithms derived from the calibration runs, and from use of ECAL channels outside the acceptance for Compton scattering.

The curves in Fig. 10 are from a preliminary simulation of the experiment that generated Fig. 1 as well. The simulation includes both nonlinear Compton scattering and multiple Compton scattering, which are calculated to have roughly equal rates under the condition of the experiment. Although the electron-energy spectra from these two processes are slightly different they are not readily distinguished if only the scattered electron is detected. However, measurement of the spectrum of scattered photons in a second phase of the experiment can separate the two processes.

The data from the ECAL scans are replotted in Fig. 11 to reveal the nonlinear dependence on laser energy more directly. As the rates are normalized to the scattered-photon signal which is primarily ordinary Compton scat-

tering, data at electron energies dominated by order n should vary with laser pulse energy as U^{n-1}. Data for four scattered-electron energies are shown in Fig. 11 along with solid curves representing the ideal power-law behavior. The open circles are the results of the simulation of the experiment and indicate that the results are expected to deviate somewhat from a pure power law.
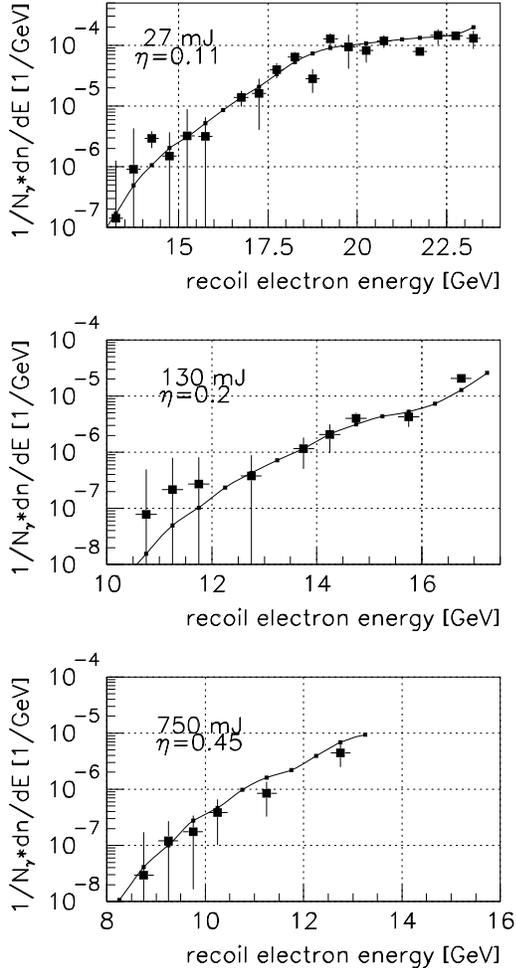

FIG. 10. Energy spectra of scattered electrons as observed in the ECAL calorimeter for 3 of 12 laser intensities. The data are normalized to the total Compton-scattered photon rate measured in the CCM1 detector. The curves are from a simulation of the experiment.

Analysis of the nonlinear Compton scattering data continues with the goal of improved understanding of systematic effects in normalization and of the effect of shower spreading in the ECAL on the rapid variation of rate with position.

We have also searched for positron production via the two-step process in which high-energy photons from Compton scattering interact within the laser focus to create an e^+e^- pair. The laser beam was frequency doubled which increased the value of Υ slightly, and permitted positron production with fewer laser photons. Indeed, with the infrared laser at least 8 laser photons

must combine with a high-energy photon to produce an e^+e^- pair, while only 4 laser photons are required for the frequency-doubled green laser. The overall rate for positron production by the green laser depends on the fifth power of the laser intensity: one power for ordinary Compton scattering to produce the high-energy photon, and four more powers to produce the pair in the photon-photon reaction. The green laser beam was linearly polarized following a conjecture that the threshold rate of pair creation in photon-photons collisions is greater for linear than circular polarization.
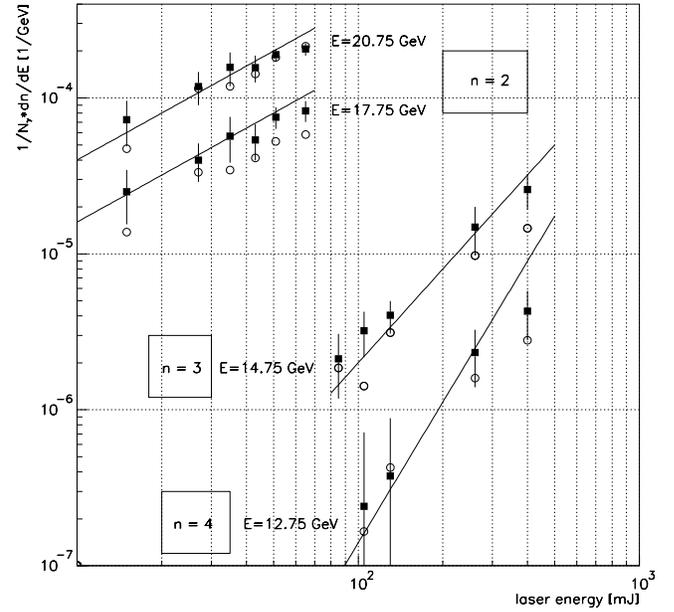

FIG. 11. The normalized rate of scattered electrons of various energies as a function of laser pulse energy (solid boxes). The open circles are from a simulation of the experiment. The solid lines represent the simple power-law expectation if the data are dominated by the lowest-order Compton scattering appropriate for the electron energy.

We used the PCAL calorimeter to search for positrons produced at IP1. Because of the high rate of electrons in the ECAL calorimeter from Compton scattering it was not possible to distinguish the electron partners of the positrons. The response of PCAL to positrons was studied by inserting an Al foil at IP1 during calibration runs to produce Bethe-Heitler e^+e^- pairs with results shown in Fig. 12a. Positrons were also produced in showers of lost electrons upstream of IP1; the rate of these background positrons was studied in 29,622 electron-beam pulses when the laser was not fired, as shown in Fig. 12b. The background positrons were deflected to slightly larger y-values by magnets upstream of IP1. From these data a signal band was defined around the proper energy/position correlation in PCAL for positron production at IP1. The 34 positrons within this band found in the laser-on pulses (Fig. 12c) are the signal candidates. Figure 12d shows the signal-candidate positrons in laser-on (solid line) and laser-off (dashed line) events

as a function of energy, where the laser-off results have been scaled by $6,068/29,622 = 0.2$. The scaled background rate is consistent with 1.6 positrons per energy bin, which rate has been subtracted from the laser-on candidates to produce the signal spectrum shown in Fig. 12e.
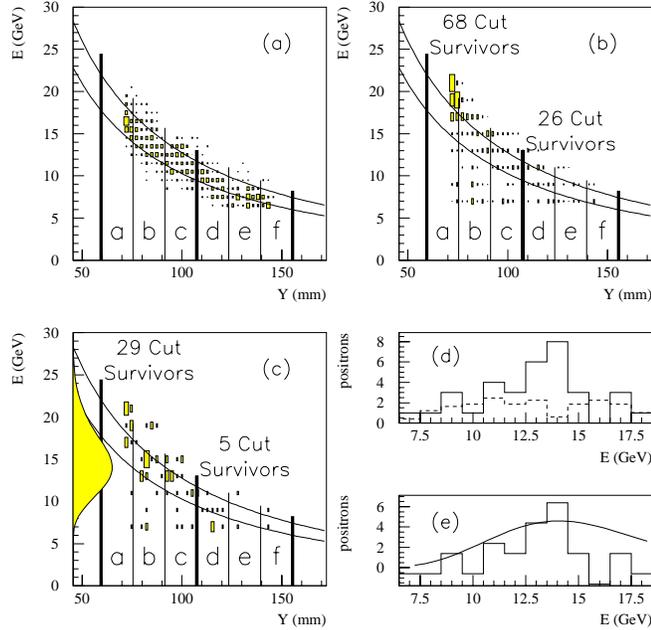

FIG. 12. Energy *vs.* position distribution of positrons observed in the PCAL when (a) an Al foil is inserted at IP1; (b) the laser is off; (c) the laser is on. The curving bands in (a)-(c) define the search region for positrons produced at IP1. The spectrum plotted along the vertical axis of (c) is from a simulation of multiphoton pair creation at IP1. (d) The IP1-positron candidates from (b) (dashed line) and (c) (solid line) as a function of energy; the background candidates from (b) have been scaled down by 0.2. (e) The signal of positrons produced at IP1 obtained by subtracting 1.6 background positrons per 2-GeV bin from the laser-on candidates; the smooth curve is the simulated spectrum also shown in (c).

The curve in Figs. 12c and 12e is from a simulation of the expected positron spectrum; very little signal is expected or found for energies below 10 GeV (rows d-f of PCAL). Using only PCAL rows a-c to quantify the signal, we find 15.1 ± 5.6 positrons in the laser-on data above the background. This signal is the first evidence for a light-by-light scattering process with real photons only, and in particular with optical photons.

---

[1] G.A. Schott, *Electromagnetic Radiation*, (Cambridge University Press, 1912).

[2] T.J. Englert and E.A. Rinehart, Phys. Rev. A **28**, 1539 (1983).

[3] See, for example, M. Billardon *et al.*, J. de Phys., Colloq. **44**, C1 (1983).

[4] D.M. Volkov, Z. Phys. **94**, 250 (1935).

[5] See also V.B. Berestetskii *et al.*, *Quantum Electrodynamics*, 2nd ed., (Pergamon Press, 1982), §40.

[6] N.D. Sengupta, Bull. Math. Soc. (Calcutta) **44**, 175 (1952).

[7] L.S. Brown and T.W.B. Kibble, Phys. Rev. **133**, A705 (1964).

[8] A.I. Nikishov and V.I. Ritus, Sov. Phys. JETP **19**, 529, 1191 (1964); **20**, 757 (1965); see also §101 of ref. [5].

[9] I.I. Gol'dman, Sov. Phys. JETP **19**, 954 (1964); Phys. Lett. **8**, 103 (1964).

[10] N.B. Narozhny *et al.*, Sov. Phys. JETP **20**, 622 (1965).

[11] T.W.B. Kibble, Phys. Rev. Lett. **16**, 1054 (1966); Phys. Rev. **150**, 1060 (1966).

[12] J.H. Eberly and A. Sleeper, Phys. Rev. **176**, 1570 (1968).

[13] C.I. Moore *et al.*, Phys. Rev. Lett **74**, 2439 (1995).

[14] F. Sauter, Z. Phys. **69**, 742 (1931). See also §129, prob. 2 of ref. [5].

[15] O. Klein, Z. Phys. **53**, 157 (1929).

[16] W. Heisenberg and H. Euler, Z. Phys. **98**, 718 (1936).

[17] G. Breit and J.A. Wheeler, Phys. Rev. **46**, 1087 (1934).

[18] H.R. Reiss, J. Math. Phys. **3**, 59 (1962). Phys. Rev. Lett. **26**, 1072 (1971).

[19] M. Bell and J.S. Bell, Part. Acc. **24**, 1 (1988); R. Blankenbecler and S.D. Drell, Phys. Rev. Lett. **61**, 2324 (1988); M. Jacob and T.T. Wu, Nucl. Phys. **B303**, 373, 389 (1989); **B327**, 285 (1989); P. Chen and K. Yokoya, Phys. Rev. Lett. **61**, 1101 (1988); V.N. Baier *et al.*, Nucl. Phys. **B328**, 387 (1989); P. Chen and V.L. Telnov, Phys. Rev. Lett. **63**, 1796 (1989); R. Blankenbecler *et al.*, Phys. Rev. D **40**, 2462 (1989).

[20] I.F. Ginzburg *et al.*, Nucl. Instr. and Meth. **205**, 47 (1983).

[21] K.O. Mikaelian, Phys. Rev. D **17**, 750 (1978); **30**, 1115 (1984); I.F. Ginzburg *et al.*, Nucl. Phys. **B228**, 285 (1983).

[22] P. Chen and R.B. Palmer, SLAC-PUB-5966 (Nov. 1992).

[23] D. Strickland and G. Mourou, Opt. Comm. **55**, 447 (1985).

[24] C. Bamber *et al.*, U. Rochester preprint UR-1428 (June 1995).

[25] W.S. Martin and J.P. Chernoch, U.S. Patent 3633126 (1972).

[26] M.J.W. Rodwell *et al.*, Opt. Lett. **11**, 638 (1986).

[27] T. Kotseroglou *et al.*, submitted to Nucl. Instr. and Meth. (Aug. 1995).

[28] V. Balakin *et al.*, Phys. Rev. Lett. **74**, 2479, (1995).

[29] S.C. Berridge *et al.*, IEEE Trans. Nucl. Sci. **37**, 1191 (1990).

[30] M.B. Woods *et al.*, E144 Internal Note (Oct. 17, 1994).